Frequency-Domain Interchip Interference Cancelation for DS-CDMA Downlink Transmission

Kazuaki Takeda, *Student Member, IEEE*, and Fumiyuki Adachi, *Fellow, IEEE*

***Abstract*—The use of frequency-domain equalization (FDE) based on minimum-mean-square-error criterion can significantly improve the bit-error-rate (BER) performance of orthogonal multicode direct-sequence code-division multiple access downlink signal transmission in a frequency-selective fading channel. However, the presence of residual interchip interference (ICI) after FDE produces the orthogonality distortion among the spreading codes, and the BER performance degrades as the number of multiplex order increases. In this paper, we propose a frequency-domain ICI cancelation scheme, in which the residual ICI replica in the frequency domain is generated and subtracted from each frequency component of the received signal after FDE. Three types of ICI cancelation scheme are presented, and the effectiveness of the proposed ICI cancelation scheme is confirmed by computer simulation.**

***Index Terms*—Direct-sequence code-division multiple access (DS-CDMA), frequency-domain equalization (FDE), interchip-interference (ICI) cancelation.**

I. Introduction

THE WIRELESS channel is composed of many propagation paths with different time delays, producing frequency-selective multipath fading [1]. Direct-sequence code-division multiple access (DS-CDMA) can exploit the channel frequency selectivity by the use of coherent rake combining that resolves the propagation paths having different time delays and coherently combines them to obtain the path diversity gain [2]. Wideband DS-CDMA [3] has been adopted as a wireless access technique in third-generation (3G) mobile communication systems for data transmissions of up to a few megabits per second. Recently, demands for broadband services in mobile communication systems are increasing, and a lot of attention has been paid to the development of next-generation mobile communication systems that support much higher data rate services (e.g., higher than a few tens of megabits per second) than 3G systems [4]. However, the bit-error-rate (BER) performance of DS-CDMA with rake combining may significantly degrade due to a strong interpath interference (IPI). Hence, IPI cancelation techniques have been studied for DS-CDMA rake receivers, e.g., [5] and [6].

Manuscript received August 9, 2005; revised March 16, 2006 and May 4, 2006. The review of this paper was coordinated by Dr. M. Stojanovic.

The authors are with the Department of Electrical and Communication Engineering, Graduate School of Engineering, Tohoku University, Sendai, 980-8579, Japan (e-mail: takeda@mobile.ecei.tohoku.ac.jp; adachi@ecei.tohoku.ac.jp).

Digital Object Identifier 10.1109/TVT.2007.895474

Recently, multicarrier (MC)-CDMA has been attracting much attention in broadband wireless access [7]–[9] since it can achieve good BER performance in a severe frequency-selective channel by using a simple one-tap frequency-domain equalization (FDE) technique. MC-CDMA has the flexibility to provide multirate transmissions, yet retain multiple access capability, as DS-CDMA does. Recently, it has been shown [10]–[15] that FDE based on the minimum-mean-square-error (mmse) criterion can improve BER performance for DS-CDMA downlink signal transmission and provide almost the same performance as MC-CDMA. In [10], mmse-FDE is combined with transmit/receive antenna diversity. mmse-FDE is applied to orthogonal multicode DS-CDMA, and the transmission performance with mmse-FDE is compared with rake combining in [11]. In [12], the theoretical BER analysis of DS-CDMA with FDE is presented. The joint use of FDE and multiaccess interference (MAI) cancelation for the DS-CDMA uplink is considered in [13] and [14], and the DS-CDMA downlink performance with mmse-FDE is evaluated in [15].

Although FDE can significantly improve BER performance of DS-CDMA, the presence of residual interchip interference (ICI) after FDE degrades the BER performance. If the residual ICI is sufficiently suppressed, BER performance approaches the matched filter bound. In [16], time-domain adaptive decision feedback equalization (DFE) based on mmse criterion is proposed for DS-CDMA. In [17], an iterated-decision equalizer is presented to reduce the effect of intersymbol interference for single-carrier transmission. In [18], frequency-domain iterative block DFE is presented for SC transmission. In [17] and [18], the computation of the correlation between the transmitted symbol and detected symbol is required and must be estimated. Furthermore, [17] and [18] consider only the nonspread SC transmission (i.e., SF $= 1$) and assume the single-user case. In this paper, we consider the orthogonal multicode DS-CDMA downlink signal transmission, where different users' spread chip sequences are code multiplexed. Therefore, in the orthogonal multicode DS-CDMA downlink, if the ICI is present after FDE, the orthogonality distortion among users is produced by the residual ICI, and this degrades the BER performance as the number of multiplex order increases. In this paper, we propose frequency-domain ICI cancelation for the DS-CDMA downlink using mmse- and maximum ratio combining (MRC)-FDE. MRC-FDE enhances the residual ICI due to the frequency selectivity of the channel. However, it can provide the largest signal-to-noise power ratio (SNR). This advantage of

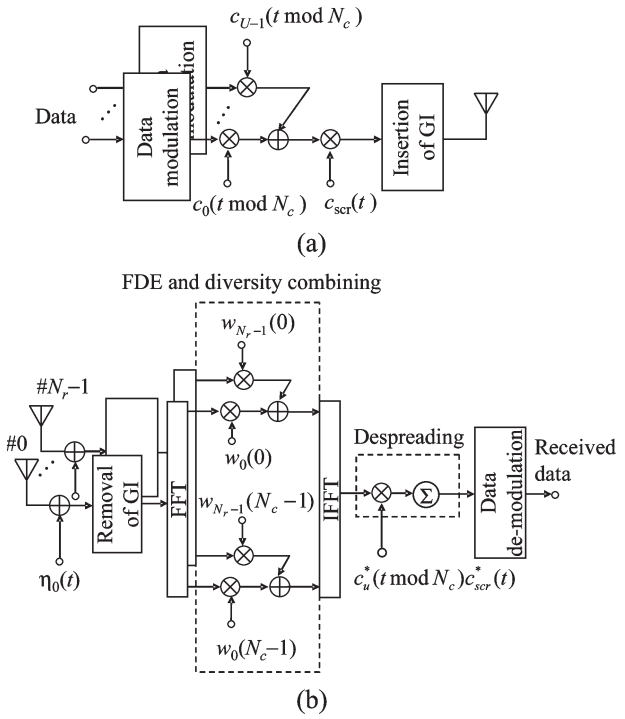

Fig. 1. Transmission system model for DS-CDMA downlink with joint FDE and antenna diversity. (a) Base station transmitter and (b) mobile receiver (uth user).

MRC-FDE is exploited by the proposed ICI cancelation. In the proposed scheme, mmse-FDE is first performed to obtain an accurate frequency-domain ICI replica. Then, the ICI replica is subtracted from the MRC-FDE output to suppress the residual ICI and gain the largest SNR. With the proposed ICI cancelation, the orthogonality distortion among users is restored after suppressing the residual ICI.

The remainder of this paper is organized as follows. Section II shows that the presence of residual ICI degrades the BER performance of the DS-CDMA downlink with FDE. In Section III, the proposed frequency-domain ICI cancelation is presented. In Section IV, the achievable BER performance in a frequency-selective Rayleigh fading channel is evaluated by computer simulation, and the effect of the proposed ICI cancelation is discussed. Section V offers some conclusions.

II. FDE and Residual ICI

A. Overall Transmission System Model

The transmission system model for DS-CDMA downlink with joint FDE and antenna diversity is illustrated in Fig. 1. The difference in the transmitter/receiver structure between MC-CDMA and DS-CDMA is just as follows: Fast Fourier transform (FFT) and inverse FFT (IFFT) are used at the MC-CDMA transmitter and receiver, respectively, while both are used at the DS-CDMA receiver. At the base station transmitter, the uth user's binary data sequence $u = 0 \sim (U-1)$ is transformed into data modulated symbol sequence $\{d_u(n)\}$ and then spread by multiplying an orthogonal spreading sequence $c_u(t)$. The resultant U chip sequences are multiplexed and further multiplied by a common scramble sequence $c_{\rm scr}(t)$ to make the resultant multicode DS-CDMA signal white-noise like. Then, the orthogonal multicode DS-CDMA signal is divided into a sequence of blocks of N_c chips each, and then, the last N_g chips of each block are copied as a cyclic prefix and inserted into the guard interval (GI) at the beginning of each block, as illustrated in Fig. 2.

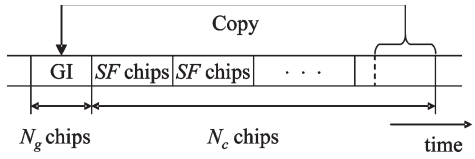

Fig. 2. Block structure.

The GI-inserted orthogonal multicode DS-CDMA signal is transmitted from the base station over a frequency-selective fading channel and is received by N_r antennas of the uth user mobile station. After the removal of the GI, the received signal on each antenna is decomposed by N_c-point FFT into N_c subcarrier components (the terminology "subcarrier" is used for explanation purposes only, although subcarrier modulation is not used). Then, joint FDE and antenna diversity combining is carried out in the frequency domain [12]. Finally, IFFT is applied to obtain the time-domain received spread signal for despreading and data demodulation.

B. Transmit and Received Signals

Throughout this paper, chip-spaced time representation of transmitted signals is used. Without loss of generality, a transmission of U data symbol sequences $\{d_u(n); u = 0 \sim U-1, n = 0 \sim (N_c/\mathrm{SF}-1)\}$ is considered, where N_c and SF are chosen so that the value of N_c/SF becomes an integer. The spread signal $\{\hat{s}(t); t = -N_g \sim (N_c-1)\}$, which is to be transmitted after the GI insertion, can be expressed, using the equivalent lowpass representation as

$$\hat{s}(t) = \sqrt{2E_c/T_c}\, s(t \bmod N_c) \tag{1}$$

where E_c and T_c denote the chip energy and the chip duration, respectively, and $s(t)$ is given by

$$s(t) = \left[\sum_{u=0}^{U-1} d_u\left(\lfloor t/\mathrm{SF} \rfloor\right) c_u(t \bmod \mathrm{SF})\right] c_{\rm scr}(t) \tag{2}$$

with $|d_u(n)| = |c_u(t)| = |c_{\rm scr}(t)| = 1$ for $t = 0 \sim (N_c-1)$, where $\lfloor x \rfloor$ represents the largest integer smaller than or equal to x.

The propagation channel is assumed to be a frequency-selective block fading channel having chip-spaced L discrete paths, each subjected to independent fading. The assumption of block fading means that the path gains remain constant over at least one block duration. The channel impulse response $h_m(t)$ observed by the mth receive antenna can be expressed as [19]

$$h_m(t) = \sum_{l=0}^{L-1} h_{m,l}\,\delta(t-\tau_l) \tag{3}$$

where $h_{m,l}$ and τ_l are the complex-valued path gain and time delay of the lth path $(l = 0 \sim (L-1))$, respectively, with $\sum_{l=0}^{L-1} E[|h_{m,l}|^2] = 1$ ($E[\cdot]$ denotes the ensemble average operation). The received signal $\{r_m(t); t = -N_g \sim (N_c-1)\}$ on the mth antenna $m = 0 \sim (N_r - 1)$ can be expressed as

$$r_m(t) = \sum_{l=0}^{L-1} h_{m,l}\hat{s}(t-\tau_l) + \eta_m(t) \tag{4}$$

where $\eta_m(t)$ is a zero-mean complex Gaussian process with a variance of $2N_0/T_c$ with N_0 being the single-sided power spectrum density of the additive white Gaussian noise (AWGN) process.

C. Joint FDE and Antenna Diversity Combining

After the removal of the GI from the received signal $r_m(t)$, an N_c-point FFT is applied to decompose $\{r_m(t); t = 0 \sim (N_c-1)\}$ into N_c subcarrier components $\{R_m(k); k = 0 \sim (N_c-1)\}$. The kth subcarrier component $R_m(k)$ can be written as

$$\begin{aligned} R_m(k) &= \sum_{t=0}^{N_c-1} r_m(t)\exp\left(-j2\pi k\frac{t}{N_c}\right) \\ &= \sqrt{\frac{2E_c}{T_c}}H_m(k)S(k) + \Pi_m(k) \end{aligned} \tag{5}$$

where $S(k)$, $H_m(k)$, and $\Pi_m(k)$ are the kth subcarrier component of the transmitted signal $\{s(t); t = 0 \sim (N_c-1)\}$, the channel gain, and the noise component due to the AWGN, respectively. They are given by

$$\begin{cases} S(k) = \sum\limits_{t=0}^{N_c-1} s(t)\exp\left(-j2\pi k\frac{t}{N_c}\right) \\ H_m(k) = \sum\limits_{l=0}^{L-1} h_{m,l}\exp\left(-j2\pi k\frac{\tau_l}{N_c}\right) \\ \Pi_m(k) = \sum\limits_{t=0}^{N_c-1} \eta_m(t)\exp\left(-j2\pi k\frac{t}{N_c}\right) \end{cases}. \tag{6}$$

Then, joint FDE and antenna diversity combining is carried out as

$$\begin{aligned} \hat{R}(k) &= \sum_{m=0}^{N_r-1} R_m(k)w_m(k) \\ &= \sqrt{\frac{2E_c}{T_c}}S(k)\hat{H}(k) + \hat{\Pi}(k) \end{aligned} \tag{7}$$

with

$$\begin{cases} \hat{H}(k) = \sum\limits_{m=0}^{N_r-1} w_m(k)H_m(k) \\ \hat{\Pi}(k) = \sum\limits_{m=0}^{N_r-1} w_m(k)\Pi_m(k) \end{cases} \tag{8}$$

where $w_m(k)$ is the equalization weight, and $\hat{H}(k)$ and $\hat{\Pi}(k)$ are the equivalent channel gain and the noise component after joint FDE and antenna diversity combining, respectively. We consider mmse- and MRC-FDE. The MRC weight realizes a matched filter to the channel and maximizes the SNR at each subcarrier. The mmse weight is chosen so that the mean square error (mse) between $S(k)$ and $\hat{R}(k)$ is minimized. The equalization weight for joint FDE and antenna diversity combining is given by [12]

$$w_m(k) = \begin{cases} \dfrac{H_m^*(k)}{\sum\limits_{m=0}^{N_r-1}|H_m(k)|^2 + \left(\frac{U}{\mathrm{SF}}\frac{E_s}{N_0}\right)^{-1}}, & \text{for mmse-FDE} \\ H_m^*(k), & \text{for MRC-FDE} \end{cases} \tag{9}$$

where E_s/N_0 is the average symbol energy-to-AWGN power spectrum density ratio, and * denotes the complex conjugation operation. Notice that the same mmse weight can be used in DS- and MC-CDMA [12].

D. Despreading and Data Demodulation

N_c-point IFFT is applied to transform the frequency-domain signal $\{\hat{R}(k); k = 0 \sim (N_c-1)\}$ into the time-domain signal $\{\hat{r}(t); t = 0 \sim (N_c-1)\}$:

$$\begin{aligned} \hat{r}(t) &= \frac{1}{N_c}\sum_{k=0}^{N_c-1}\hat{R}(k)\exp\left(j2\pi t\frac{k}{N_c}\right) \\ &= \sqrt{\frac{2E_c}{T_c}}\left(\frac{1}{N_c}\sum_{k=0}^{N_c-1}\hat{H}(k)\right)s(t) + \mu(t) + \hat{\eta}(t) \end{aligned} \tag{10}$$

where $s(t)$ in the first term represents the transmitted chip, $\mu(t)$ is the residual ICI component, and $\hat{\eta}(t)$ is the noise component. $\mu(t)$ and $\hat{\eta}(t)$ can be expressed as

$$\begin{cases} \mu(t) = \sqrt{\frac{2E_c}{T_c}}\frac{1}{N_c}\sum\limits_{k=0}^{N_c-1}\hat{H}(k)\left[\sum\limits_{\substack{\tau=0 \\ \neq t}}^{N_c-1} s(\tau)\exp\left(j2\pi k\frac{t-\tau}{N_c}\right)\right] \\ \hat{\eta}(t) = \frac{1}{N_c}\sum\limits_{k=0}^{N_c-1}\hat{\Pi}(k)\exp\left(j2\pi k\frac{t}{N_c}\right) \end{cases}. \tag{11}$$

Note that if $\hat{H}(k) \neq$ constant, $\mu(t) \neq 0$ (the ICI cannot be removed). Despreading is carried out on $\hat{r}(t)$ to obtain the uth user's decision variable for data demodulation on $d_u(n)$, giving

$$\hat{d}_u(n) = \frac{1}{\mathrm{SF}}\sum_{t=n\mathrm{SF}}^{(n+1)\mathrm{SF}-1}\hat{r}(t)c_u^*(t \bmod \mathrm{SF})c_{\mathrm{scr}}^*(t). \tag{12}$$

Substitution of (10) and (11) into (12) gives

$$\hat{d}_u(n) = \sqrt{\frac{2E_c}{T_c}}\left(\frac{1}{N_c}\sum_{k=0}^{N_c-1}\hat{H}(k)\right)d_u(n) + \overline{\mu}(n) + \overline{\eta}(n) \tag{13}$$

TABLE I
SIMULATION PARAMETERS

Transmitter	Modulation	QPSK
	Number of FFT points	N_c=256
	GI	N_g=32(chip)
	Spreading sequence	Product of Walsh sequence and PN sequence
	Spreading factor	SF=16
Channel	Fading	Frequency -selective block Rayleigh fading
	Power delay profile	L=16-path uniform power delay profile
Receiver	Number of receive antennas	N_r=1,2
	Frequency-domain equalization	MRC, MMSE
	Channel estimation	Ideal

where $\overline{\mu}(n)$ and $\overline{\eta}(n)$ are given by

$$\begin{cases} \overline{\mu}(n) = \frac{1}{\mathrm{SF}} \sum\limits_{t=n\mathrm{SF}}^{(n+1)\mathrm{SF}-1} c^*(t) \\ \qquad \times \left[\frac{1}{N_c} \sum\limits_{k=0}^{N_c-1} \hat{H}(k) \left\{ \sqrt{\frac{2E_c}{T_c}} \sum\limits_{\substack{\tau=0 \\ \neq t}}^{N_c-1} s(\tau) \exp\left(j2\pi k \frac{t-\tau}{N_c} \right) \right\} \right] \\ \overline{\eta}(n) = \frac{1}{\mathrm{SF}} \sum\limits_{t=n\mathrm{SF}}^{(n+1)\mathrm{SF}-1} c^*(t) \left\{ \frac{1}{N_c} \sum\limits_{k=0}^{N_c-1} \hat{\Pi}(k) \exp\left(j2\pi t \frac{k}{N_c} \right) \right\} \end{cases} \tag{14}$$

and their variances are obtained by

$$\begin{cases} 2\sigma_{\mathrm{ICI}}^2 = E[|\mu_{\mathrm{ICI}}|^2] \\ \qquad = 2\frac{U}{\mathrm{SF}} \frac{E_c}{T_c} \left[\frac{1}{N_c} \sum\limits_{k=0}^{N_c-1} \left| \hat{H}(k) \right|^2 - \left| \frac{1}{N_c} \sum\limits_{k=0}^{N_c-1} \hat{H}(k) \right|^2 \right]. \\ 2\sigma_{\mathrm{noise}}^2 = E[|\mu_{\mathrm{noise}}|^2] \\ \qquad = 2\frac{1}{\mathrm{SF}} \frac{N_0}{T_c} \left(\frac{1}{N_c} \sum\limits_{k=0}^{N_c-1} \sum\limits_{m=0}^{N_r-1} |w_m(k)|^2 \right) \end{cases} \tag{15}$$

E. Impact of Residual ICI on BER Performance

It is clearly understood from (13) that the frequency diversity gain can be obtained by FDE. The first term in (13) is the desired symbol component. $\overline{H} = (1/N_c) \sum_{k=0}^{N_c-1} \hat{H}(k)$ is equivalent to the channel gain in a frequency-nonselective channel. The probability that $\overline{H}$ drops (or fades) is very small compared with the frequency-nonselective channel case since $\overline{H}$ is the average of N_c different equivalent channel gains. However, the residual ICI causes the orthogonality distortion among the spreading codes and may degrade the achievable BER performance in a frequency-selective fading channel (i.e., $\hat{H}(k) \neq$ constant) as the code multiplex order increases. The impact of the residual ICI on the BER performance is evaluated by computer simulation. The simulation parameters are summarized in Table I. We assume quaternary phase-shift keying (QPSK) data modulation, FFT block size of $N_c = 256$ chips, and a GI of $N_g = 32$ chips. The fading channel is assumed to be a frequency-selective block Rayleigh fading channel having a chip-spaced L-path uniform power delay profile (i.e., $\mathrm{E}[|h_{m,l}|^2] = 1/L$ for all m and l), and the normalized maximum Doppler frequency $f_{\mathrm{D}}T_c(N_c + N_g) = 0.001$, where $f_{\mathrm{D}} = \nu/\lambda$ with ν and λ represent, respectively, the mobile terminal traveling speed and the carrier frequency ($f_{\mathrm{D}}T_c(N_c + N_g) = 0.001$ corresponds to a traveling speed of $\nu = 75$ km/h for a chip rate of $1/T_c = 100$ MHz, 5-GHz carrier frequency, $N_c = 256$, and $N_g = 32$). Perfect chip timing and ideal channel estimation are assumed.

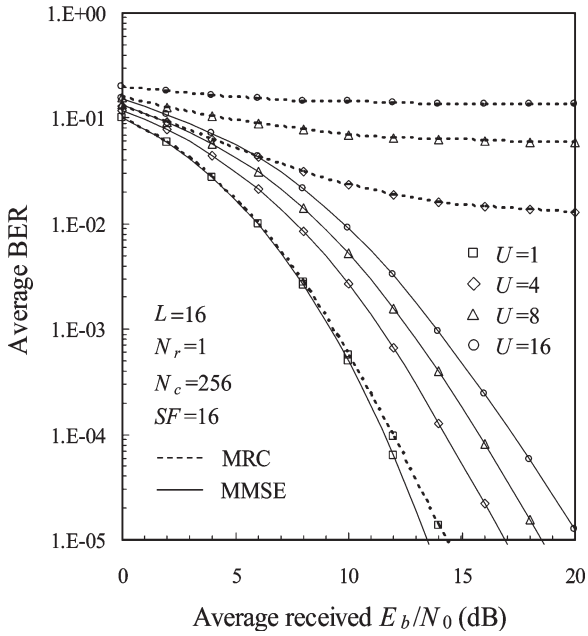

Fig. 3. Downlink BER performance with mmse-FDE and MRC-FDE.

The simulated BER performance with mmse and MRC-FDE is plotted in Fig. 3 as a function of the average received signal energy per bit-to-AWGN power spectrum density ratio E_b/N_0, given by $E_b/N_0 = \mathrm{SF}(1 + N_g/N_c)(E_c/N_0)$, when $N_r = 1$ (no antenna diversity) and $\mathrm{SF} = 16$. Decision errors are caused by the residual ICI and the AWGN. The former becomes the predominant cause of decision errors in high E_b/N_0 regions and produces the BER floor (since the amount of residual ICI depends on the channel frequency-selectivity but not on the E_b/N_0 value). When $U = 1$, the mmse- and MRC-FDE can achieve almost the same BER performance. However, when $U \geq 4$, the BER floors are seen with MRC-FDE due to a larger orthogonality distortion caused by the residual ICI; mmse-FDE can always achieve better BER performance than MRC, and no BER floors are seen. However, although mmse-FDE provides much better BER performance than MRC, its BER performance degrades as U becomes larger.

III. ICI CANCELATION

It has been shown in Section II that the performance degradation is due to the orthogonality distortion caused by the residual ICI. ICI cancelation can be introduced in FDE to improve BER

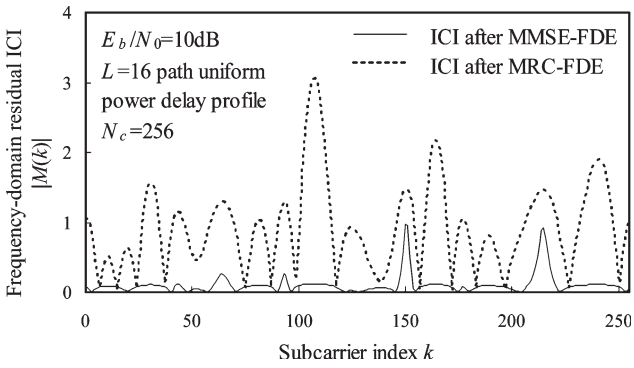

Fig. 4. One-shot observation of the residual ICI.

performance. In this section, a mathematical expression for the residual ICI is presented first, and then, frequency-domain ICI cancelation is proposed.

A. Frequency-Domain Representation of Residual ICI

An N_c-point FFT is applied to $\{\mu(t); t = 0 \sim (N_c - 1)\}$ in (11) to obtain the residual ICI components $\{M(k); k = 0 \sim (N_c - 1)\}$ in the frequency-domain. $M(k)$ is given by

$$M(k) = \sqrt{\frac{2E_c}{T_c}} \left\{ \hat{H}(k) - \frac{1}{N_c} \sum_{k'=0}^{N_c-1} \hat{H}(k') \right\} S(k). \quad (16)$$

Using (16), the one-shot observation of the residual ICI in the frequency-domain is plotted in Fig. 4. As understood from (16), the frequency-domain residual ICI is proportionate to the difference between the equivalent channel gain $\hat{H}(k)$ and its average. It can be seen from Fig. 4 that the residual ICI after mmse-FDE is very small since $\hat{H}(k)$ is almost flat over the entire frequency range. On the other hand, large residual ICI is seen for MRC-FDE due to the enhanced frequency-selectivity of the equivalent channel after equalization.

B. ICI Cancelation

The receiver structure using the proposed frequency-domain ICI cancelation is illustrated in Fig. 5. We consider three types of ICI cancelation using mmse-FDE and MRC-FDE. Type I, II, and III canceler structures are illustrated in Fig. 6. $\hat{R}(k)$ in (7), after joint mmse-FDE and diversity combining, is denoted by $\hat{R}_{\mathrm{mmse}}(k)$, and $\hat{R}(k)$, after joint MRC-FDE and diversity combining, is denoted by $\hat{R}_{\mathrm{MRC}}(k)$. The type I cancelation scheme uses only $\hat{R}_{\mathrm{mmse}}(k)$, as shown in Fig. 6(a). On the other hand, the type II and type III cancelation schemes make use of both $\hat{R}_{\mathrm{mmse}}(k)$ and $\hat{R}_{\mathrm{MRC}}(k)$, as shown in Fig. 6(b) and (c). Without ICI cancelation, mmse-FDE gives a better BER performance than MRC-FDE, as stated in Section II. Hence, for all types of ICI cancelation, mmse-FDE is first performed to obtain a more accurate ICI replica for ICI cancelation. However, if the residual ICI is perfectly canceled, MRC-FDE gives a better BER performance than mmse-FDE since MRC-FDE yields a higher SNR. Therefore, the MRC-FDE output is used in the type II and III schemes to gain the highest SNR after suppressing the residual ICI by ICI cancelation.

1) Type I: The type I cancelation scheme consists of two steps. The $i = 0$th step uses the output $\hat{R}_{\mathrm{mmse}}(k)$ of joint mmse-FDE and diversity combining. An N_c-point IFFT is applied to $\{\hat{R}_{\mathrm{mmse}}(k); k = 0 \sim (N_c - 1)\}$ in order to obtain the time-domain chip sequence $\hat{r}^{(0)}_{\mathrm{mmse}}(t)$ [which corresponds to $\hat{r}(t)$ in (10)]. After the despreading of $\hat{r}^{(0)}_{\mathrm{mmse}}(t)$ as in (12), the soft decision symbol replica $\widetilde{d}_u(n)$ is generated as

$$\widetilde{d}_u(n) = \frac{1}{\sqrt{2}} \tanh\left(\chi \mathrm{Re}\left[\frac{\hat{d}_u(n)}{\sqrt{2E_c/T_c}} \right] \right) + j\frac{1}{\sqrt{2}} \tanh\left(\chi \mathrm{Im}\left[\frac{\hat{d}_u(n)}{\sqrt{2E_c/T_c}} \right] \right) \quad (17)$$

for QPSK data modulation, where $\tanh(x)$ is given by

$$\tanh(x) = \frac{\exp(x) - \exp(-x)}{\exp(x) + \exp(-x)} \quad (18)$$

and χ is a parameter that controls the extent to which the soft decision contributes to the replica generation. When $\chi \to \infty$, (17) represents a hard decision. On the other hand, when $\chi = 0$, (17) always gives $\widetilde{d}_u(n) = 0$, and hence, this represents the case without ICI cancelation.

After the respreading of $\widetilde{d}_u(n)$ for $u = 0 \sim U - 1$, U chip sequences are multiplexed and further multiplied by the common scramble sequence $c_{\mathrm{scr}}(t)$ used at the base station transmitter. Then, chip interleaving is used to generate the replica $\widetilde{s}^{(0)}(t)$ corresponding to the spread signal $s(t)$ transmitted from the base station. Respreading of erroneous symbol replica produces error propagation over consecutive SF chips. To avoid this, chip interleaving is used at both the transmitter and receiver (the chip-interleaver is described in Section IV).

After chip interleaving, the N_c-point FFT is applied to decompose the replica $\widetilde{s}^{(0)}(t)$ into N_c subcarrier components. The kth subcarrier component $\widetilde{S}^{(0)}(k)$ is given by

$$\widetilde{S}^{(0)}(k) = \sum_{t=0}^{N_c-1} \widetilde{s}^{(0)}(t) \exp\left(-j2\pi k \frac{t}{N_c} \right). \quad (19)$$

The ICI replica $\tilde{M}^{(0)}_{\mathrm{mmse}}(k)$ is generated by substituting $\widetilde{S}^{(0)}(k)$ into (16) in the $i = 1$st step. It is then subtracted from $\hat{R}_{\mathrm{mmse}}(k)$. The signal components $\widetilde{R}^{(1)}(k)$, after ICI cancelation, is given by

$$\widetilde{R}^{(1)}(k) = \hat{R}_{\mathrm{mmse}}(k) - \tilde{M}^{(0)}_{\mathrm{mmse}}(k) \quad (20)$$

where $\tilde{M}^{(0)}_{\mathrm{mmse}}(k)$ is given by

$$\tilde{M}^{(0)}_{\mathrm{mmse}}(k) = \sqrt{\frac{2E_c}{T_c}} \left\{ \hat{H}_{\mathrm{mmse}}(k) - \frac{1}{N_c} \sum_{k'=0}^{N_c-1} \hat{H}_{\mathrm{mmse}}(k') \right\} \widetilde{S}^{(0)}(k) \quad (21)$$

with $\hat{H}_{\mathrm{mmse}}(k)$ being obtained from (8) using the mmse weight.

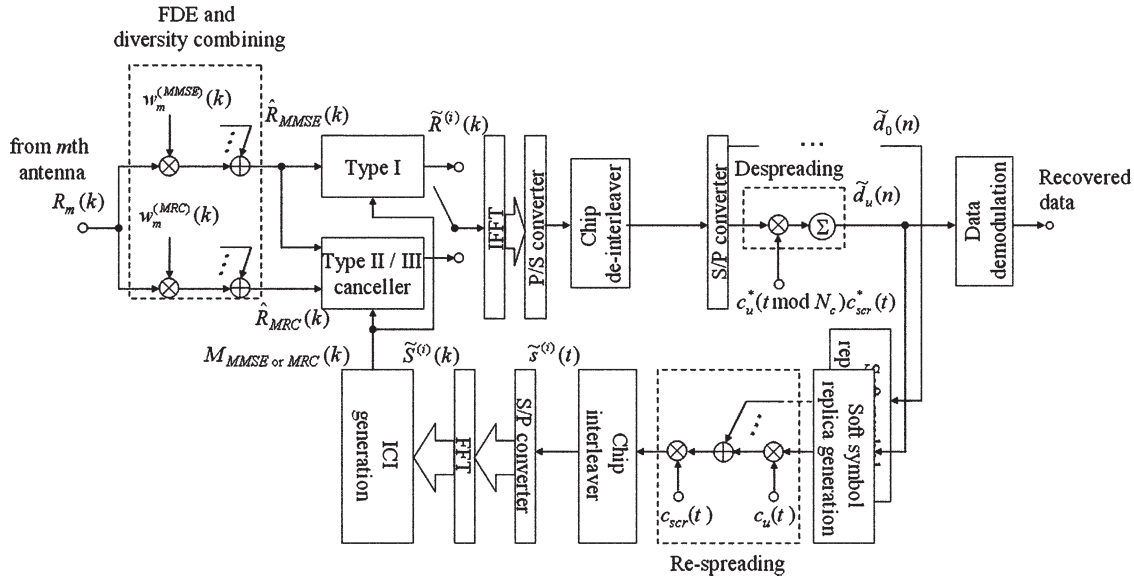

Fig. 5. Receiver structure using frequency-domain ICI cancelation for the uth user.

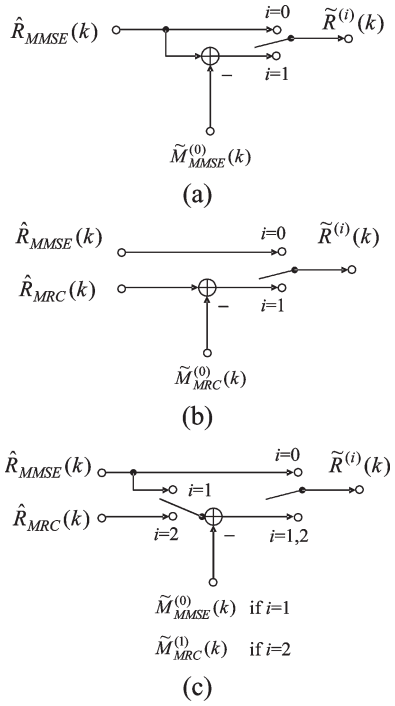

Fig. 6. ICI cancelation structure. (a) Type I. (b) Type II. (c) Type III.

Finally, a series of N_c-point IFFT operation, chip-deinterleaving, despreading, and data-demodulation is carried out again to recover the transmitted data.

2) Type II: The type II cancelation scheme is comprised of two steps. As shown in Fig. 6(b), the $i = 0$th step uses the output $\hat{R}_{\mathrm{mmse}}(k)$ of joint mmse-FDE and diversity combining. N_c-point IFFT is applied to $\{\hat{R}_{\mathrm{mmse}}(k); k = 0 \sim (N_c - 1)\}$ to obtain the time-domain signal $\hat{r}^{(0)}_{\mathrm{mmse}}(t)$. After the despreading of $\hat{r}^{(0)}_{\mathrm{mmse}}(t)$, the soft decision symbol replica $\widetilde{d}_u(n)$ is generated for $u = 0 \sim (U - 1)$, as in (17). After the respreading of $\widetilde{d}_u(n)$, U parallel chip sequences are multiplexed and further multiplied by $c_{\mathrm{scr}}(t)$. Then, chip interleaving is used to generate the replica $\widetilde{s}^{(0)}(t)$ of the spread signal $s(t)$ transmitted from the base station. After chip-interleaving, the N_c-point FFT is applied to decompose the replica $\widetilde{s}^{(0)}(t)$ into N_c subcarrier components $\widetilde{S}^{(0)}(k)$, as in (19). The above $i = 0$th step of type II cancelation is the same as that of type I cancelation.

What makes type II cancelation different from type I cancelation is the $i = 1$st step, i.e., the ICI replica $\tilde{M}^{(0)}_{\mathrm{MRC}}(k)$ is generated and subtracted from $\hat{R}_{\mathrm{MRC}}(k)$ [see Fig. 6(b)]. Hence, the signal component $\tilde{R}^{(1)}(k)$ is given by

$$\widetilde{R}^{(1)}(k) = \hat{R}_{\mathrm{MRC}}(k) - \tilde{M}^{(0)}_{\mathrm{MRC}}(k) \tag{22}$$

where $\tilde{M}^{(0)}_{\mathrm{MRC}}(k)$ is generated using (21) but replacing $\hat{H}_{\mathrm{mmse}}(k)$ by $\hat{H}_{\mathrm{MRC}}(k)$. The type II cancelation scheme maximizes the SNR after the ICI cancelation if the symbol replica generation is correct [i.e., $\widetilde{S}^{(0)}(k) = S(k)$ for all k in (19)].

3) Type III: The type III cancelation scheme is comprised of three steps [see Fig. 6(c)]. The $i = 0$th step and $i = 1$st step are the same as in type I. After performing type I cancelation, the symbol replica $\widetilde{s}^{(1)}(t)$, which is more reliable than $\widetilde{s}^{(0)}(t)$, is generated and decomposed into $\widetilde{S}^{(1)}(k)$ by N_c-point FFT. Then, in the $i = 2$nd step, the ICI replica $\tilde{M}^{(1)}_{\mathrm{MRC}}(k)$ is generated and subtracted from $\hat{R}_{\mathrm{MRC}}(k)$. $\tilde{R}^{(i)}(k)$ for type III is given by

$$\tilde{R}^{(i)}(k) = \begin{cases} \hat{R}_{\mathrm{mmse}}(k) - \tilde{M}^{(0)}_{\mathrm{mmse}}(k), & \text{for } i = 1 \quad \text{(type I)} \\ \hat{R}_{\mathrm{MRC}}(k) - \tilde{M}^{(1)}_{\mathrm{MRC}}(k), & \text{for } i = 2 \end{cases} \tag{23}$$

where

$$\tilde{M}^{(1)}_{\mathrm{MRC}}(k) = \sqrt{\frac{2E_c}{T_c}} \left\{ \hat{H}_{\mathrm{MRC}}(k) - \frac{1}{N_c} \sum_{k'=0}^{N_c-1} \hat{H}_{\mathrm{MRC}}(k') \right\} \widetilde{S}^{(1)}(k) \tag{24}$$

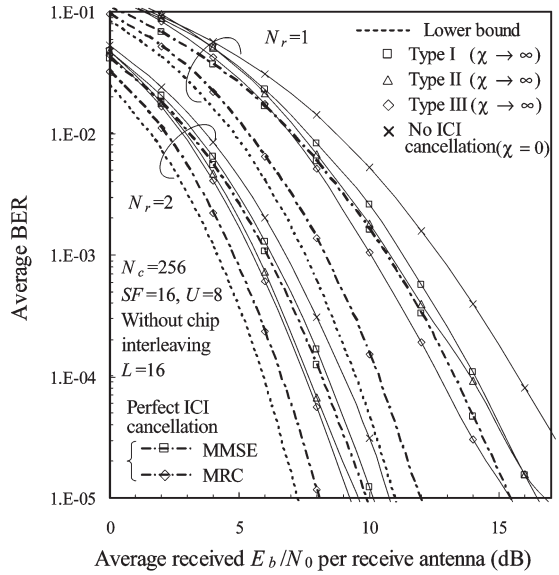

(a)

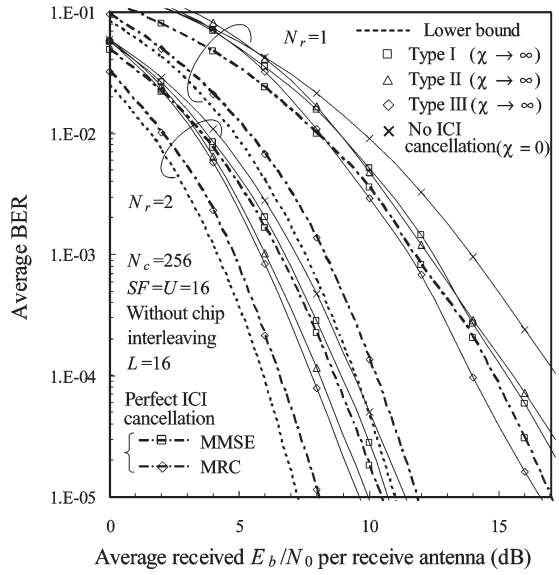

(b)

Fig. 7. Downlink BER performance with hard ICI cancelation ($\chi \to \infty$) without chip interleaving. (a) $U = 8$, (b) $U = 16$.

with

$$\widetilde{S}^{(1)}(k) = \sum_{t=0}^{N_c-1} \widetilde{s}^{(1)}(t) \exp\left(-j2\pi k \frac{t}{N_c}\right). \qquad (25)$$

IV. Computer Simulation

The simulation parameters are the same as in Table I. We first discuss the effect of hard ICI cancelation [i.e., $\chi \to \infty$ in (17)] and then the effect of soft ICI cancelation.

A. Hard ICI Cancelation

The downlink BER performance with hard ICI cancelation ($\chi \to \infty$) and without chip interleaving is plotted in Fig. 7 as a function of the average received E_b/N_0 for SF $= 16$. For comparison, the performance using mmse-FDE without ICI cancelation [i.e., $\chi \to 0$ in (17)] and the BER performances of mmse-FDE and MRC-FDE with perfect ICI cancelation are also plotted in Fig. 7. The theoretical lower bound is also plotted in Fig. 7 to show how the BER performance improves if the residual ICI can be perfectly canceled. The theoretical lower bound is given by [2]

$$P_{b,\mathrm{MF\ bound}}(\Gamma) = \left[\frac{1}{2}\left(1 - \sqrt{\frac{\Gamma/2}{\Gamma/2+L}}\right)\right]^L \sum_{k=0}^{L-1} \binom{L-1+k}{k} \times \left[\frac{1}{2}\left(1+\sqrt{\frac{\Gamma/2}{\Gamma/2+L}}\right)\right]^k \qquad (26)$$

where $\binom{a}{b}$ is the binomial coefficient, and $\Gamma = \mathrm{SF}(E_c/N_0)$ is the average signal energy per symbol-to-AWGN power spectrum density ratio E_s/N_0. Note that if the residual ICI is perfectly canceled, the orthogonality among users can be restored, and the MAI is not produced; therefore, the MAI effect is not considered in (26).

It can be seen from Fig. 7 that if the residual ICI is perfectly canceled, MRC-FDE provides better BER performance than mmse-FDE since MRC-FDE achieves a higher SNR. This implies that the type II and III cancelation schemes using both mmse- and MRC-FDE give better BER performance than the type I cancelation scheme using mmse-FDE only. This performance superiority of the type II and III cancelation schemes to the type I cancelation scheme can be confirmed from Fig. 7; however, the type I cancelation scheme can improve BER performance and approaches mmse-FDE with perfect ICI cancelation. It is seen that the type III cancelation scheme can further improve BER performance compared with the type II cancelation scheme. This is because the type III cancelation scheme uses, for ICI replica generation, the ICI-reduced signal obtained by the type I cancelation scheme.

The downlink BER performance for $U = 8$ is plotted in Fig. 7(a). With the type III cancelation scheme, an E_b/N_0 reduction of about 3 dB is achieved for BER $= 10^{-4}$ from the case without cancelation, but the performance degradation from the theoretical lower bound is still 3.3 dB (including a 0.5-dB loss due to the GI insertion). The use of two-branch ($N_r = 2$) antenna diversity combining is effective to further improve BER performance. The type III cancelation scheme with antenna diversity provides a BER performance close to the lower bound by about 1.6 dB. The downlink BER performance for $U = 16$ is illustrated in Fig. 7(b). The achievable BER performance is worse than the case of $U = 8$ since the larger orthogonality distortion among the spreading codes is produced due to the residual ICI for $U = 16$. With the type III cancelation scheme, an E_b/N_0 reduction of about 3.2 dB is achieved from the case without cancelation.

So far, we have considered the case without chip interleaving, in which respreading of an erroneous symbol replica produces the error propagation over consecutive SF chips, thereby generating unreliable ICI replica. The chip interleaving

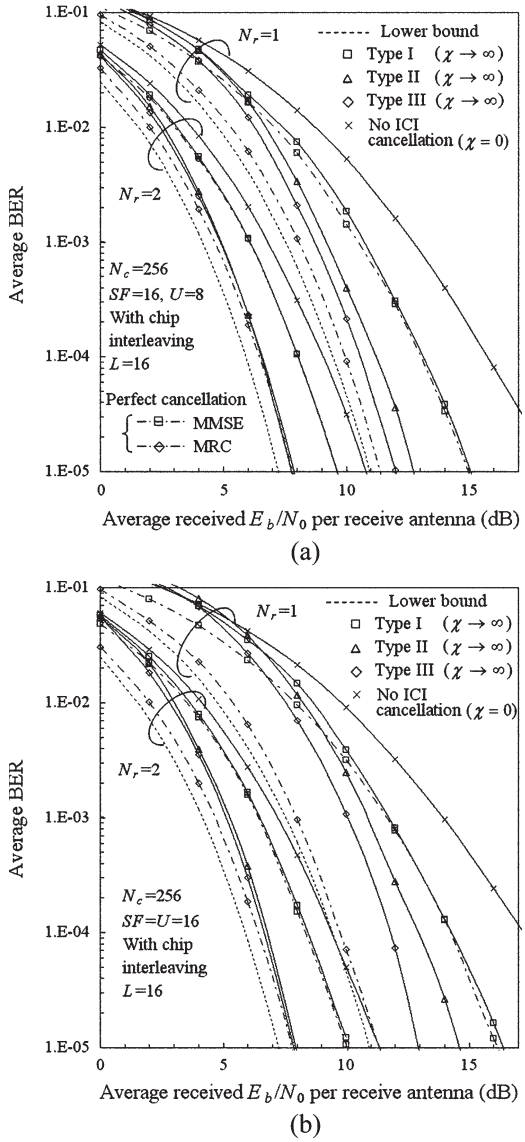

Fig. 8. Downlink BER performance with hard ICI cancelation ($\chi \to \infty$) and chip interleaving. (a) $U = 8$, (b) $U = 16$.

technique can be used to avoid this error propagation and further improve downlink BER performance. In this paper, the SF $\times N_c$ row–column interleaver is used as a chip interleaver. The effect of chip interleaving is shown in Fig. 8(a) and (b) for the case of $U = 8$ and 16, respectively. The use of chip interleaving provides a better BER performance than the case without chip interleaving. This is because a more reliable ICI replica can be generated by the use of chip interleaving. Similar to the case without chip interleaving, the type III cancelation scheme provides a better BER performance than the type I and II schemes. When $U = 8$ (16), the required E_b/N_0 for BER $= 10^{-4}$ can be reduced with the type III cancelation scheme by as much as about 5.1 (5.4) dB from the case without cancelation. The BER performance for $U = 8$ (16) approaches the lower bound by about 1.2 (2.4) dB when $N_r = 1$. When $N_r = 2$ and $U = 8$ (16), the BER performance with the type III scheme approaches the lower bound by about 0.7 (0.8) dB (including a 0.5-dB loss due to the GI insertion).

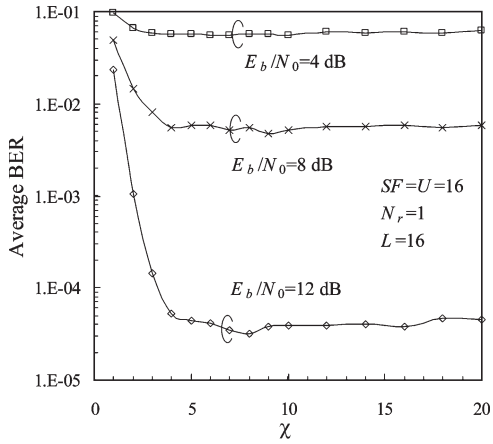

Fig. 9. Dependency of BER achievable by type III soft ICI cancelation on χ for SF $= U = 16$ and $N_r = 1$.

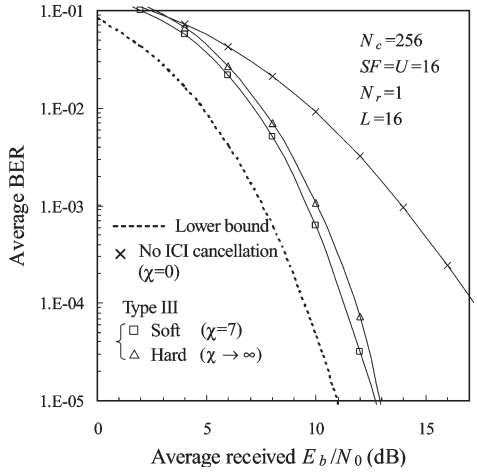

Fig. 10. Performance comparison of type III soft ICI cancelation and hard decision ICI cancelation when SF $= U = 16$ and $N_r = 1$.

B. Soft ICI Cancelation

So far, we have assumed hard ICI cancelation ($\chi \to \infty$), but the use of soft symbol replica generation reduces the influence of error propagation. The BER dependence on χ with the type III soft ICI cancelation scheme is plotted in Fig. 9 for $N_r = 1$ when SF $= U = 16$. When $\chi \to 0$, the soft decision symbol replica becomes 0, and therefore, the BER performance with $\chi \to 0$ approaches that without ICI cancelation. On the other hand, when $\chi \to \infty$, the soft decision symbol replica approaches the hard decision symbol replica; in this case, decision error produces large interference due to error propagation and, hence, degrades BER performance. Therefore, there is an optimum value of χ. It is seen that there is a broad optimum of χ that gives the smallest BER for each E_b/N_0 value. However, the optimum χ is almost independent of E_b/N_0 and can be taken as $\chi = 7$. Therefore, in the following simulation, $\chi = 7$ is used.

Fig. 10 compares the downlink BER performances with the type III soft and hard ICI cancelation schemes for $N_r = 1$ when SF $= U = 16$. For comparison, the performance without ICI cancelation and the theoretical lower bound are also plotted. The use of the soft symbol replica provides a better BER

performance. An E_b/N_0 reduction of about 0.5 dB is achieved with soft ICI cancelation for BER $= 10^{-4}$, and the BER performance with the type III soft ICI cancelation scheme approaches the theoretical lower bound by 1.9 dB, even if $N_r = 1$.

V. Conclusion

The residual ICI after FDE degrades the BER performance of DS-CDMA downlink signal transmission with FDE. In this paper, in order to suppress the residual ICI, frequency-domain ICI cancelation was proposed, and the downlink BER performance in a frequency-selective Rayleigh fading channel was evaluated by computer simulation. In the proposed frequency-domain ICI cancelation, the ICI replica in the frequency-domain is generated and subtracted from each subcarrier component after FDE. Three types of ICI cancelation scheme have been presented in this paper. Type III uses the ICI-reduced chip sequence obtained by the type I cancelation scheme to improve the reliability of ICI replica, thereby achieving the best BER performance. It was shown that the joint use of chip interleaving is beneficial to alleviate the error propagation effect and improve the reliability of the ICI replica generation. When the number U of users is $U = 8$ (16) for SF $= 16$, the E_b/N_0 reduction for BER $= 10^{-4}$ from the case without cancelation was found to be about 5.1 (5.4) dB. The use of two-branch antenna diversity brings the BER performance close to the theoretical lower bound by about 0.8 dB when $U = 16$. The effect of soft and hard ICI cancelation was also discussed. It was shown that the use of soft ICI cancelation improves the achievable BER performance by about 0.5 dB for $U = 16$.

References

[1] *Microwave Mobile Communications*, W. C. Jakes, Jr., Ed. New York: Wiley, 1974.

[2] J. G. Proakis, *Digital Communications*, 3rd ed. New York: McGraw-Hill, 1995.

[3] F. Adachi, M. Sawahashi, and H. Suda, "Wideband DS-CDMA for next generation mobile communications systems," *IEEE Commun. Mag.*, vol. 36, no. 9, pp. 56–69, Sep. 1998.

[4] Y. Kim *et al.*, "Beyond 3G: Vision, requirements, and enabling technologies," *IEEE Commun. Mag.*, vol. 41, no. 3, pp. 120–124, Mar. 2003.

[5] K. Higuchi, K. Okawa, M. Sawahashi, and F. Adachi, "Field experiments on pilot symbol-assisted coherent multistage interference canceller in DS-CDMA reverse link," *IEICE Trans. Commun.*, vol. E86-B, no. 1, pp. 191–205, Jan. 2003.

[6] S. Moshavi, "Multi-user detection for DS-CDMA communications," *IEEE Commun. Mag.*, vol. 34, no. 10, pp. 124–136, Oct. 1996.

[7] S. Hara and R. Prasad, "Overview of multicarrier CDMA," *IEEE Commun. Mag.*, vol. 35, no. 12, pp. 126–144, Dec. 1997.

[8] M. Helard, R. Le Gouable, J.-F. Helard, and J.-Y. Baudais, "Multicarrier CDMA techniques for future wideband wireless networks," *Ann. Telecommun.*, vol. 56, no. 5/6, pp. 260–274, 2001.

[9] H. Atarashi, S. Abeta, and M. Sawahashi, "Variable spreading orthogonal frequency and code division multiplexing (VSF-OFCDM) for broadband packet wireless access," *IEICE Trans. Commun.*, vol. E86-B, no. 1, pp. 291–299, Jan. 2003.

[10] F. W. Vook, T. A. Thomas, and K. L. Baum, "Cyclic-prefix CDMA with antenna diversity," in *Proc. IEEE VTC—Spring*, May 2002, pp. 1002–1006.

[11] F. Adachi, T. Sao, and T. Itagaki, "Performance of multicode DS-CDMA using frequency domain equalization in a frequency selective fading channel," *Electron. Lett.*, vol. 39, no. 2, pp. 239–241, Jan. 2003.

[12] F. Adachi and K. Takeda, "Bit error rate analysis of DS-CDMA with joint frequency-domain equalization and antenna diversity combining," *IEICE Trans. Commun.*, vol. E87-B, no. 10, pp. 2991–3002, Oct. 2004.

[13] S. Tomasin and N. Benvenuto, "Equalization and multiuser interference cancellation in CDMA systems," in *Proc. 6th Int. Symp. WPMC*, Yokosuka, Japan, Oct. 19–22, 2003, vol. 1, pp. 10–14.

[14] S. Tomasin and N. Benvenuto, "Frequency-domain interference cancellation and nonlinear equalization for CDMA systems," *IEEE Trans. Wireless Commun.*, vol. 4, no. 5, pp. 2329–2339, Sep. 2005.

[15] I. Martoyo, G. M. A. Sessler, J. Luber, and F. K. Jondral, "Comparing equalizers and multiuser detections for DS-CDMA downlink systems," in *Proc. IEEE VTC—Spring*, May 2004, pp. 1649–1653.

[16] L.-M. Chen and B.-S. Chen, "A robust adaptive DFE receiver for DS-CDMA systems under multipath fading channels," *IEEE Trans. Commun.*, vol. 49, no. 7, pp. 1523–1532, Jul. 2001.

[17] A. M. Chan and G. W. Wornell, "A class of block-iterative equalizers for intersymbol interference channels: Fixed channel results," *IEEE Trans. Commun.*, vol. 49, no. 11, pp. 1966–1976, Nov. 2001.

[18] N. Benvenuto and S. Tomasin, "Block iterative DFE for single carrier modulation," *Electron. Lett.*, vol. 38, no. 19, pp. 1144–1145, Sep. 2002.

[19] T. S. Rappaport, *Wireless Communications*. Englewood Cliffs, NJ: Prentice-Hall, 1996.

Kazuaki Takeda (S'03) received the B.E. and M.S. degrees in communications engineering from Tohoku University, Sendai, Japan, in 2003 and 2004, respectively, where he is currently working toward the Ph.D. degree with the Department of Electrical and Communications Engineering, Graduate School of Engineering.

His research interests include equalization, interference cancelation, transmit/receive diversity, and multiple access techniques.

Mr. Takeda was a recipient of the 2003 Institute of Electronics, Information, and Communication Engineers of Japan (IEICE) Radio Communication Systems Active Research Award, and the 2004 Inose Scientific Encouragement Prize.

Fumiyuki Adachi (M'79–SM'90–F'02) received the B.S. and Dr. Eng. degrees in electrical engineering from Tohoku University, Sendai, Japan, in 1973 and 1984, respectively.

In April 1973, he was with the Electrical Communications Laboratories of Nippon Telegraph and Telephone Corporation (now NTT) and conducted various types of research related to digital cellular mobile communications. From July 1992 to December 1999, he was with NTT Mobile Communications Network, Inc. (now NTT DoCoMo, Inc.), where he led a research group on wideband/broadband CDMA wireless access for IMT-2000 and beyond. Since January 2000, he has been with Tohoku University, where he is a Professor of electrical and communication engineering at the Graduate School of Engineering. His research interests are in CDMA wireless access techniques, equalization, transmit/receive antenna diversity, multiple-input multiple-output, adaptive transmission, and channel coding, with particular application to broadband wireless communications systems. From October 1984 to September 1985, he was a United Kingdom Science and Engineering Council Visiting Research Fellow with the Department of Electrical Engineering and Electronics, Liverpool University, Liverpool, U.K.

Dr. Adachi served as a Guest Editor of the IEEE Journal on Selected Areas in Communications on Broadband Wireless Techniques (October 1999), Wideband CDMA I (August 2000), Wideband CDMA II (January 2001), and Next Generation CDMA Technologies (January 2006). He was a corecipient of the IEEE Vehicular Technology Transactions Best Paper of the Year Award in 1980 and 1990 as well as a recipient of the Avant Garde Award in 2000. He is a member of Institute of Electronics, Information, and Communication Engineers of Japan (IEICE), was a recipient of the IEICE Achievement Award in 2002, and a corecipient of the IEICE Transactions Best Paper of the Year Award in 1996 and 1998. He was a recipient of Thomson Scientific Research Front Award in 2004.